

54th SME North American Manufacturing Research Conference (NAMRC 54, 2026)

Near-Field Perception for Safety Enhancement of Autonomous Mobile Robots in Manufacturing Environments

Li-Wei Shih^{a,1}, Ruo-Syuan Mei^{a,1}, Jesse Heidrich^b, Hui-Ping Wang^b, Joel Hooton^b, Joshua Solomon^b, Jorge Arinez^c, Guangze Li^{c,*}, Chenhui Shao^{a,*}

^aDepartment of Mechanical Engineering, University of Michigan, MI 48109, USA

^bManufacturing Technology Development, General Motors R&D, Warren, MI 48092, USA

^cMaterials & Manufacturing Systems Research, General Motors R&D, Warren, MI 48092, USA

Abstract

Near-field perception is essential for the safe operation of autonomous mobile robots (AMRs) in manufacturing environments. Conventional ranging sensors such as light detection and ranging (LiDAR) and ultrasonic devices provide broad situational awareness but often fail to detect small objects near the robot base. To address this limitation, this paper presents a three-tier near-field perception framework. The first approach employs light-discontinuity detection, which projects a laser stripe across the near-field zone and identifies interruptions in the stripe to perform fast, binary cutoff sensing for obstacle presence. The second approach utilizes light-displacement measurement to estimate object height by analyzing the geometric displacement of a projected stripe in the camera image, which provides quantitative obstacle height information with minimal computational overhead. The third approach employs a computer vision-based object detection model on embedded AI hardware to classify objects, enabling semantic perception and context-aware safety decisions. All methods are implemented on a Raspberry Pi 5 system, achieving real-time performance at 25 or 50 frames per second. Experimental evaluation and comparative analysis demonstrate that the proposed hierarchy balances precision, computation, and cost, thereby providing a scalable perception solution for enabling safe operations of AMRs in manufacturing environments.

© 2026 The Authors. Published by Elsevier Ltd. This is an open access article under the CC BY-NC-ND license (<http://creativecommons.org/licenses/by-nc-nd/4.0/>)

Peer-review under responsibility of the scientific committee of the NAMRI/SME.

Keywords: Near-field perception; Autonomous mobile robot; Safety; Object detection; Computer vision; Smart manufacturing

1. Introduction

Autonomous mobile robots (AMRs) are now commonly used in manufacturing for material transport, parts staging, and line-side delivery in manufacturing [1, 2, 3]. They move through dynamic, human-shared spaces [4, 5, 6], so perception and decision making close to the robot are central to productivity and safety. As deployments scale, plants expect AMRs

to operate reliably across cluttered aisles, mixed lighting, and changing floor conditions [7, 8].

Many safety-critical interactions occur within the first half meter around the AMR chassis, where small components, dropped tools, cables, and human limbs can appear unexpectedly. In general, safety monitoring for AMRs, particularly in manufacturing environments, has been investigated only to a limited extent. A related but distinct application area is autonomous driving, where various sensing modalities, including 3D point clouds and ultrasonic waves, have been explored. For example, light detection and ranging (LiDAR)-based perception has been widely explored for autonomous navigation. A 3D obstacle-detection and tracking framework for mobile vehicles was developed in [9], showing strong performance in dynamic environments. A real-time LiDAR-camera fusion method was

* Corresponding authors: Guangze Li (guangze.li@gm.com), Chenhui Shao (chshao@umich.edu).

¹ These authors contributed equally to this work.

presented in [10], which improved detection accuracy through multimodal sensing. Ultrasonic sensing has also been investigated in related studies. For instance, the Simultaneous Calibration and Navigation (SCAN) framework proposed in [11] enabled precise localization and mapping in multi-sensor robot setups using multiple ultrasonic local positioning systems. Nesti et al. [12] used multiple ultrasonic transducers mounted on a vehicle bumper for short-range object detection, though the approach was limited by coarse angular resolution and difficulty distinguishing object types.

Despite these advances, existing methods developed for autonomous driving primarily address mid- to long-range perception and do not provide sufficient precision for near-field safety, which is critical in human-robot shared environments [1]. Moreover, such approaches offer only global situational awareness and often lack the spatial resolution and low latency required to detect subtle or low-profile obstacles near the robot base. Therefore, reliable near-field perception tailored to AMRs is critically needed to prevent collisions and enable responsive motion planning in shared work environments.

To meet this need, this paper proposes a hierarchical three-tier framework consisting of three complementary approaches designed to balance speed, precision, and interpretability in near-field perception for AMRs. The first approach, a light-discontinuity detection method, enables rapid binary cutoff detection by identifying interruptions in a projected laser stripe, providing an immediate safety response when an obstacle is present. The second approach, a light-displacement-based height estimation method, estimates object height through the geometric shift of the projected stripe in the image plane. This allows the system to distinguish between small debris and larger obstacles. The third approach, a computer vision-based object-detection method enhanced by synthetic data generation for limited near-field perception data availability, introduces semantic understanding by classifying detected objects into predefined categories. With this information, the AMR can execute context-specific actions based on object type and associated risk. Experimental evaluation validated the effectiveness of all three approaches: the first achieved reliable obstacle detection across common industrial objects, the second demonstrated an average height estimation error of 17.8 mm (RMSE) for representative samples, and the third achieved 100% mAP@0.5 accuracy in object classification. Together, these approaches form a progressive structure that evolves from geometric to semantic perception, adaptable to a range of industrial requirements in diverse manufacturing environments.

To the best of the authors' knowledge, this is the first study to systematically investigate near-field perception for AMRs through a set of complementary geometric and semantic sensing approaches. The developed methods are implemented on an affordable Raspberry Pi 5 platform and experimentally evaluated for detection accuracy, latency, and hardware cost. Finally, a comparative analysis identifies cost-performance trade-offs and practical considerations for deploying near-field perception in manufacturing environments.

The remainder of this paper is organized as follows. Section 2 outlines the problem definition and hardware layout of the sensing system. Section 3 presents the light-cutoff detection approach. Section 4 describes the light-displacement height estimation method. Section 5 introduces the object-detection approach and its deployment on embedded hardware. Section 6 evaluates the cost, time efficiency, and limitations, and discusses potential future extensions of the proposed three-tier approaches. Finally, Section 7 summarizes the key findings and concluding remarks.

2. Method overview

This section introduces the overall architecture of the proposed near-field perception framework. The system integrates low-cost sensing modules around the AMR perimeter to detect nearby obstacles and classify potential hazards. The following subsections describe the hardware configuration, the predefined object-response logic, and the hierarchical sensing strategy that links all three approaches within a unified framework.

2.1. System setup and hardware layout

Figure 1 presents the top-view schematic of the hardware configuration for the near-field perception system. The AMR footprint (blue region) has a characteristic length denoted by d_{AMR} , while the surrounding detection zone (green region) extends outward by a distance d_{NF} . This zone is partitioned into eight monitoring regions, labeled A through H, distributed along the four sides of the robot perimeter. Each side is equipped with a Raspberry Pi camera module and a laser warning light, where each camera-light pair monitors two adjacent regions. For instance, the bottom-left module monitors regions B and C, while the bottom-right module monitors regions D and E. The integration of multiple camera-light module pairs minimizes blind spots and enhances system reliability, ensuring trustworthy co-existence with human operators on the factory floor.

2.2. Action table

To ensure consistent and safe behavior in dynamic manufacturing environments, a predefined action table is established to translate near-field detections into appropriate robot responses. Table 1 summarizes the predefined response strategy for objects detected in the near-field zone. Objects are categorized into *large* (≥ 50 mm) and *small* (< 50 mm) groups across seven classes: human, tools, materials, parts, vehicles, plant infrastructure, and safety items. The AMR operates in three possible response modes: (1) run over, (2) stop and warn, and (3) go around, depending on the object's size, category, and potential risk to human operators or equipment. The specific response triggered depends on the level of perceptual intelligence available, allowing the AMR to react based on object presence, geometric size, or semantic category.

Table 1. Action table defining AMR behavior according to object type and size

Category	Large object (≥ 50 mm)	Small object (< 50 mm)	System action
Human	Hand, foot, knee, leg, sitting or fallen operator	—	Stop
Tools	Power drill, wrench, hammer, screw-driver	Nuts, bolts, washers, markers, gloves	Continue (small); Stop or Reroute (large)
Materials	Boxes, pallets, wooden planks, containers	Paper, tape, plastic film, straps	Continue (small); Stop (large)
Parts	Trim panels, metal brackets, extrusions	Clips, fasteners, connectors	Stop
Vehicles	Forklift, cart, other AMRs	—	Stop or Reroute
Environment	Cables, cones, pipes, signage	Chair/table legs, portable devices	Stop
Safety / PPE	Barrier, cone, heavy PPE item	Safety glasses, gloves, jackets	Stop or Reroute

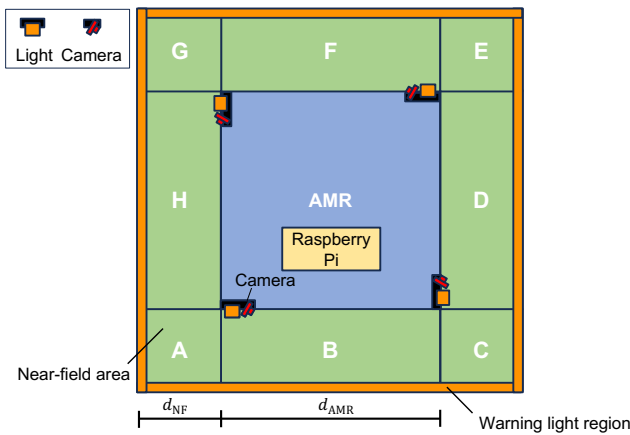


Figure 1. Top-view schematic of the AMR showing the near-field detection layout. The AMR footprint (d_{AMR}) is surrounded by a near-field detection range (d_{NF}) and a safety buffer zone illuminated by warning lights.

This action logic follows a hierarchical safety protocol: detections associated with human presence trigger immediate stops, whereas small non-hazardous debris is ignored to maintain operational efficiency. Objects classified as structural or mobile obstacles initiate a stop-and-warn response, allowing the robot to either reroute or await operator confirmation. This rule-based framework provides a balance between safety assurance and continuous navigation for AMR operations in manufacturing environments.

2.3. Overview of the three-tier perception strategy

Using the hardware configuration described in Section 2.1, three solutions for near-field perception are proposed, as illustrated in Figure 2 and summarized in Table 2. Approach 1, “Laser Line Cutoff Detection,” detects discontinuities in the laser beam projected across the detection zone and raises an alert when the beam is interrupted by an object. Approach 2, “Light Displacement-Based Height Estimation,” estimates object height through the relationship $h_{obj} = f(d, h_{light}, h_{cam})$,

Table 2. Overview of near-field sensing approaches, associated hardware, and key capabilities.

Approach	Hardware	Capability
1 Light cutoff detection	Laser diode, Raspberry Pi 5, camera	Detects object presence (binary).
2 Light displacement	Same as Approach 1	Estimates object height.
3 Object detection	Raspberry Pi 5, AI HAT+, camera	Recognizes object category.

where the height is calculated from the observed light displacement d , laser mounting height h_{light} , and camera mounting height h_{cam} . Approach 3, “Object Detection via Machine Vision Algorithm,” employs computer vision algorithms to identify specific object types (e.g., hands, feet, scissors) and generates detection decisions based on object classification. These three approaches progressively enhance detection intelligence from simple presence detection to geometric estimation and ultimately to semantic object recognition. The following sections present detailed implementation and evaluation of each solution.

3. Approach 1: laser line cutoff detection

Approach 1 identifies the presence of obstacles within the near-field zone through detecting interruptions in a projected light stripe. This binary detection mechanism serves as the foundation of the three-tier hierarchy by providing rapid, low-latency awareness of any object crossing the safety boundary. The method’s simplicity enables real-time implementation with minimal hardware cost and computation.

3.1. Light projection setup

A 653 nm laser diode is mounted on one side of the AMR. The laser beam has a rated power of 5 mW, which classifies it as a Class 3R device. Figure 3 shows the laser setup. The laser is tilted downward to cover the full detection length. However,

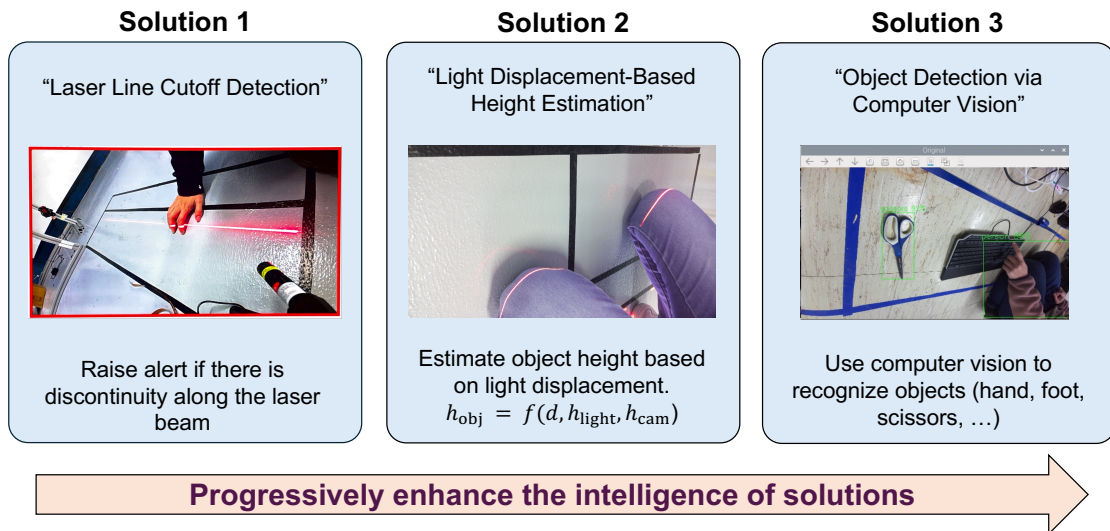


Figure 2. Overview of the three proposed near-field perception approaches.

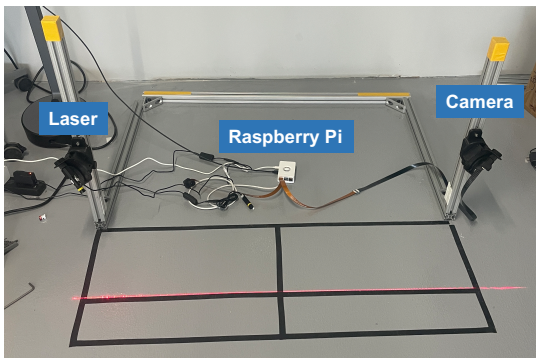


Figure 3. Hardware setup for approach 1. The laser and camera are mounted on an adjustable fixture.

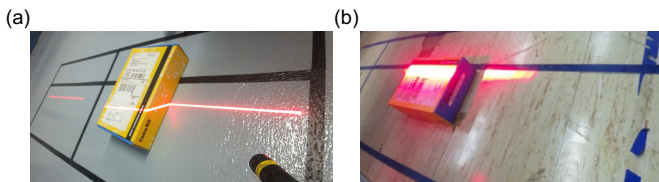


Figure 4. Comparison of illumination patterns for (a) laser-based and (b) LED-based light projection.

because of the limited vertical space available for installation, a centrally mounted laser cannot fully cover the required detection range. Mounting the laser on one side resolves this limitation but introduces a drawback: the far end of the projected beam is farther from the source, causing the stripe to appear blurred and wider compared with the near end. This effect requires additional compensation in the detection algorithm.

In cases where a Class 3R laser is not permitted, an alternative red-light LED can be used. Figure 4 compares the laser-based and LED-based approaches. The LED projects a broader

and less intense illumination pattern on the floor, which complicates segmentation. The reduced contrast between the illuminated region and the background makes it more challenging to separate the light band from the surrounding surface, particularly when the floor or nearby objects have similar color tones.

3.2. Vision system

A Raspberry Pi 5 is selected as the processing unit for this system, offering a balance of low cost and high performance suitable for embedded vision tasks. The system employs a Raspberry Pi Camera Module 3 operating at a resolution of 2304×1296 pixels and a frame rate of approximately 50 frames per second. The camera is mounted on one side of the AMR at a height of approximately 50 cm from the ground and tilted downward to capture the floor area adjacent to the robot. This downward-tilted configuration allows the camera to effectively observe the near-field zones B and C, as illustrated in Figure 1. The placement ensures complete coverage of the target detection region while maintaining compact integration with the robot chassis. This setup provides sufficient spatial detail for laser line analysis and discontinuity detection while achieving real-time performance on the Raspberry Pi 5 platform.

3.3. Line discontinuity detection algorithm

Figure 5 illustrates the proposed pipeline for Approach 1. The algorithm consists of four main stages: color thresholding, region of interest (ROI) geometry warping, spatial and temporal denoising, and continuity checking. These steps convert raw camera input into a stable binary signal that represents the presence or absence of a laser line discontinuity.

Color thresholding and line detection: To detect the projected laser stripe, the RGB image is first converted to the Hue-Saturation-Value (HSV) color space. The hue and saturation

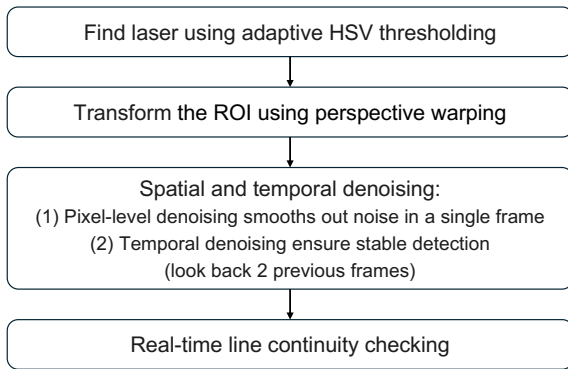


Figure 5. Processing pipeline for line cutoff detection.

tion channels are adaptively thresholded to isolate pixels corresponding to the 653 nm laser wavelength. Morphological operations remove small spurious noise. The resulting binary mask is processed using a Hough Line Transform to identify the central trajectory of the beam and estimate its orientation in the frame.

ROI geometry warping: Because the camera is mounted at an oblique angle relative to the floor, the captured image experiences perspective distortion. A homography transformation is applied to warp the region of interest into a top-down view, ensuring consistent pixel-to-millimeter scaling across the field of view. The geometric mapping parameters are obtained during calibration using a planar target with known dimensions.

Spatial and temporal denoising: Spatial denoising smooths pixel intensity variations in a single frame by applying a running average kernel corresponding to a 5 mm physical window. Temporal denoising stabilizes detection results by averaging over consecutive frames. A larger temporal window increases stability but also introduces processing delay. In this work, the current frame and two previous frames are used, which provides a balanced compromise between responsiveness and robustness. At a capture rate of 50 frames per second, this corresponds to a 20 ms delay in effective response time.

Continuity checking: The final step evaluates the continuity of the detected line along its longitudinal axis. A discontinuity is flagged when the maximum observed gap between line segments exceeds a predefined threshold specified by system safety requirements, typically five millimeters. When a discontinuity is detected, a trigger signal is sent to the decision module for immediate alerting and motion control.

3.4. Results

Approach 1 was experimentally validated using all objects listed in Table 1. Tests were performed with both single objects and mixed scenes, where multiple items were placed along the projected light line at a distance of approximately 50 cm from the AMR. Under standard laboratory lighting conditions, the system operated at 50 frames per second and generated a warning signal whenever at least one object was detected within the projected light curtain.

All tested objects, including human body parts, tools, and plant-floor components, were evaluated at four orientations (0° , 90° , 180° , and 270°) relative to the AMR. Example detection results are shown in Figure 6. In Figure 6(a), a box is placed near the projected laser stripe without making contact; the algorithm correctly ignored the shadow and produced no false alarm. In Figure 6(b), a human shoe interrupts the laser line, resulting in a positive detection. The system successfully detected all medium and large objects across all orientations. Extremely small or thin objects, such as rubber bands and narrow zip ties, were occasionally missed, particularly near the far end of the projection line where the pixel-to-millimeter resolution decreases due to perspective distortion. These undetected cases accounted for less than five percent of the total trials and occurred primarily outside the optimal detection region.

Overall, the results demonstrate that the proposed light projection setup provides robust and repeatable performance for near-field cutoff detection. The system consistently responded to the presence of both human and non-human objects while maintaining operation at 50 FPS. The slight loss of sensitivity for sub-centimeter objects in the distant region is primarily attributed to the limited pixel-to-millimeter resolution of the camera at the far end of the projection field. Future work will explore higher-resolution imaging or multi-camera configurations to improve coverage of small and thin objects.

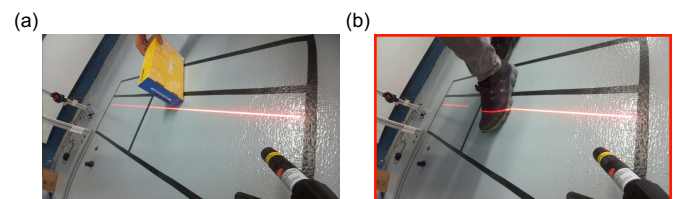


Figure 6. Example results from Approach 1, showing detection of line discontinuities when (a) no objects block the projected beam and (b) objects interrupt the projected beam.

4. Approach 2: light displacement-based height estimation

This approach extends the discontinuity detection method introduced in Section 3. Instead of only identifying the presence of an object that interrupts the projected light, the method estimates the object's height by analyzing the displacement of the projected line in the camera image. This allows precise measurement of object elevation within the near-field region, although it imposes stricter requirements on the relative placement of the camera and light source.

4.1. Height estimation

The concept of height estimation is derived from structured-light techniques commonly used in 3D scanning, where object height is determined from the geometric relationship between the camera and the projected light. A 653 nm laser line is projected across the floor, and when an object enters the detection

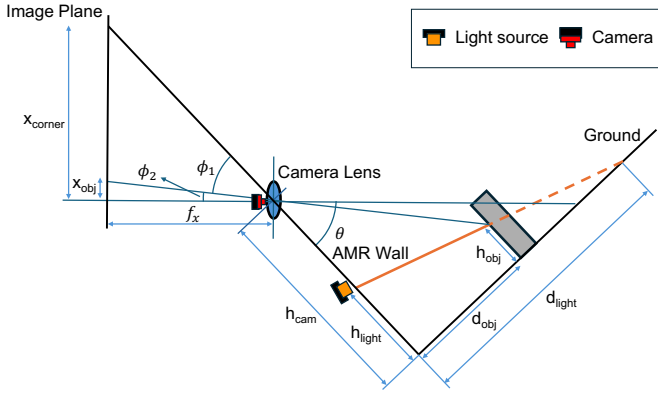


Figure 7. Geometric model of light displacement for object height estimation.

region, the illuminated stripe shifts upward in the camera image due to geometric displacement. The object height can thus be expressed as a function of the observed displacement d , laser mounting height h_{light} , and camera mounting height h_{cam} , as defined by

$$h_{\text{obj}} = f(d, h_{\text{light}}, h_{\text{cam}}). \quad (1)$$

By measuring the pixel offset between the baseline floor reference and the observed stripe, h_{obj} can be estimated through a calibrated geometric mapping. In this formulation, d_{light} and d_{obj} represent the horizontal distances from the camera to the laser source and to the detected object, respectively. The parameters x_{corner} and x_{obj} correspond to the pixel coordinates of the baseline edge and object location in the image plane, while f_x denotes the focal length in pixel units obtained from camera calibration, ensuring consistency with the image-plane measurements.

Figure 7 illustrates the geometric relationship among the camera, laser source, and object surface used for height estimation. The projected laser line forms a measurable displacement in the image plane when an object enters the detection region, and this shift corresponds to the object height through the known mounting geometry. Three governing equations are derived from these geometric relationships, as shown in Equations (2)–(4).

$$\phi_1 = \theta - \phi_2 = \tan^{-1}\left(\frac{x_{\text{corner}}}{f_x}\right) - \tan^{-1}\left(\frac{x_{\text{obj}}}{f_x}\right), \quad (2)$$

$$\frac{h_{\text{light}}}{d_{\text{light}}} = \frac{h_{\text{obj}}}{d_{\text{light}} - d_{\text{obj}}}, \quad (3)$$

$$\tan \phi_1 = \frac{d_{\text{obj}}}{h_{\text{cam}} - h_{\text{obj}}}. \quad (4)$$

By substituting Equations (3) and (4), a closed-form expression for object height is obtained:

$$h_{\text{obj}} = h_{\text{light}} \frac{d_{\text{light}} - h_{\text{cam}} \tan \phi_1}{d_{\text{light}} - h_{\text{light}} \tan \phi_1}. \quad (5)$$

Combining Equations (2) and (5) yields an analytical mapping between the observed line displacement in the image plane and the corresponding physical object height. All geometric parameters, including camera height, laser height, and projection angle, are fixed during calibration, making this formulation suitable for real-time height computation on the embedded Raspberry Pi 5 system. The resulting h_{obj} values serve as input to the near-field safety system, which differentiates small debris from taller obstacles and determines whether the robot should run over or reroute around the object.

4.2. Camera placement

Accurate height estimation through light displacement requires careful determination of the camera and laser light mounting positions and orientations. When the projected light stripe intersects an object, the magnitude of displacement observed in the camera image strongly depends on the camera's placement. A larger displacement improves measurement resolution and thus enhances the precision of height estimation.

Rather than conducting time- and labor-intensive physical adjustments in the actual system, a digital twin approach is adopted using the physics-based simulation engine [13] to model the AMR hardware configuration, as shown in Figure 8. The simulation environment replicates the AMR system using a cube geometry, with the floor plane (blue line) representing three near-field perception regions. The camera and laser light parameters, including focal length, resolution, field of view, light power, color, shape, and size, are calibrated to match the real-world hardware specifications. This digital twin enables rapid evaluation of different sensor configurations and generates synthetic images for algorithm development.

Figure 9 illustrates the rendered camera views as the camera position is varied along the y-axis and z-axis relative to the AMR edge. When the camera moves along the y-axis (positions 2, 4, and 5), the magnitude of displacement in the projected stripe remains unchanged. In contrast, shifting the camera along the z-axis (positions 1–3) produces noticeable differences: when the camera is positioned higher than the laser, the stripe shifts inward in the image, whereas when it is lower, the stripe shifts outward. The greater the vertical offset between the camera and the laser, the larger the displacement observed in the image. Consequently, to achieve higher measurement sensitivity, the camera and laser should be separated along the z-axis, while movement along the y-axis has negligible impact on displacement magnitude.

4.3. Results

The hardware setup for Approach 2 is identical to that used in Approach 1, as described in Section 3.4. Specifically, the camera is mounted at a height of 40 cm and the laser at 20 cm

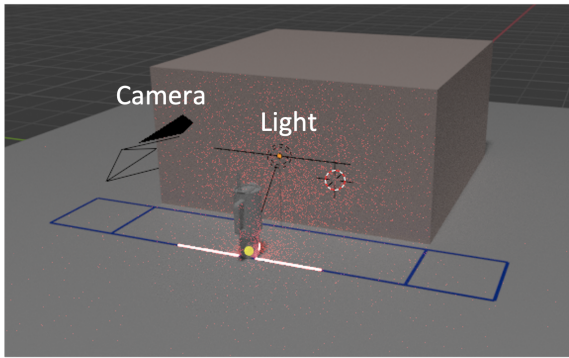


Figure 8. Digital twin in Blender used for modeling AMR geometry and testing camera–laser configurations.

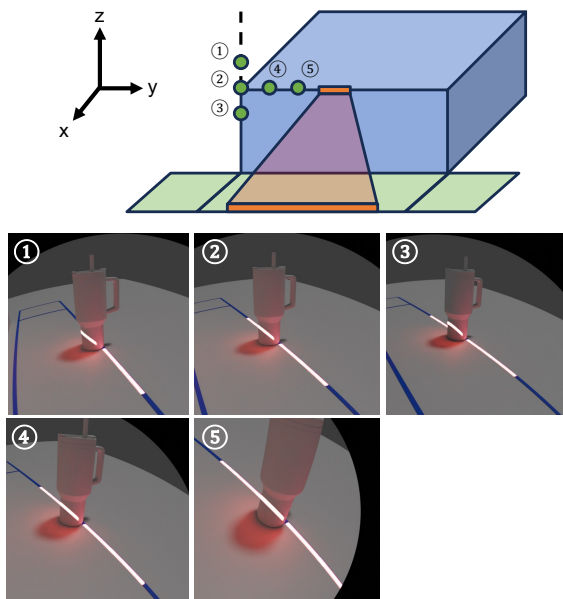


Figure 9. Evaluation of camera placement along the z-axis (positions 1–3) and y-axis (positions 2, 4, 5) relative to the AMR edge in the simulated environment.

above the floor to create a distinct light stripe across the near-field detection zone. To measure each object's height, the object was positioned such that the projected light intersected its top edge, defining the measurement point. Using the geometric formulation in Equation (5), the object height was derived from the measured pixel displacement of the projected stripe in the captured image.

The height estimation performance is summarized in Table 3. Across seven representative samples, the system achieved a root-mean-square error (RMSE) of 17.8 mm. Most deviations occurred for reflected objects such as boxes and aluminum extrusions, where the laser stripe appeared diffuse and introduced greater pixel-level uncertainty. For less diffuse surfaces, such as the knee and hand, the estimation accuracy improved to within 10 mm. Overall, the achieved accuracy is sufficient to discriminate object height categories within the near-field region, confirming that the light displacement approach effectively complements the discontinuity-based detection method.

Table 3. Height estimation results for light displacement-based approach

Object	Ground Truth (mm)	Predicted (mm)	Error (mm)
Box (1)	40	63	+23
Box (2)	60	78	+18
Box (3)	80	104	+24
Aluminum extrusion	40	59	+19
Hand	50	60	+10
Shoes	60	79	+19
Knee	120	113	−7
RMSE			17.8

Future work will focus on three dimensional model that can accommodate tilted camera angle and image processing to improving estimation on reflective objects to reduce error from height estimation.

5. Approach 3: object recognition via machine vision algorithm

The third approach introduces semantic understanding into the near-field perception. Instead of relying on geometric cues alone, a machine learning model is trained to recognize and classify factory-floor objects directly from camera images. This enables context-aware decision-making aligned with the predefined action table, allowing the AMR to distinguish between tools, materials, and human limbs.

5.1. Synthetic dataset generation

To the best of the authors' knowledge, no publicly available dataset exists for near-field object detection in manufacturing environments. As such, images of common factory floor objects were collected and overlaid onto floor plane images captured by the AMR camera to generate a synthetic dataset for model training. Synthetic data generation has increasingly been used in smart manufacturing to overcome shortages of labeled training data and to improve the robustness of computer-vision models under diverse operating conditions [14]. The synthetic data generation pipeline is illustrated in Figure 10. To improve robustness against variations in object pose and illumination, data were acquired from eight viewing angles at 45° intervals (0°–315°) for each object class (Figure 11) and under five distinct lighting conditions (Figure 12). Each object image was then segmented and background-removed, producing approximately 2,800 clean object samples across 70 unique items. In parallel, 2,000 floor images were randomly cropped from AMR video recordings to serve as backgrounds. Synthetic scenes were generated by randomly varying object number, position, and orientation on these floor images, yielding a final dataset of 5,000 synthetic images for model training and validation. This multi-angle and multi-illumination data collection strategy ensures that the trained detection model can reliably recognize objects regardless of their orientation or lighting condition within the near-field detection zone.

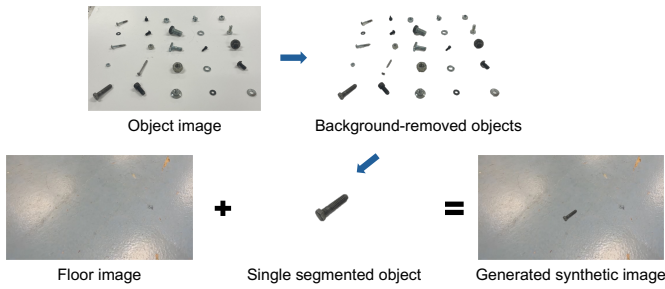


Figure 10. Synthetic dataset generation pipeline for industrial environment objects.

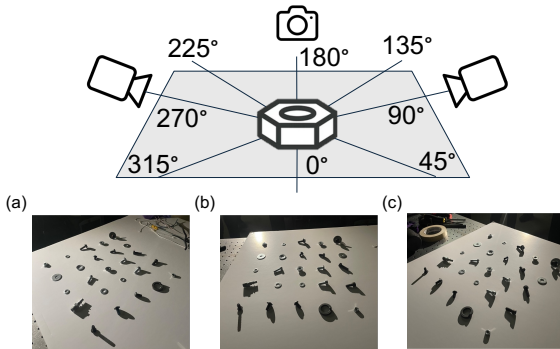


Figure 11. Example of multi-angle data acquisition from eight orientations for each object category (a) 45°, (b) 90°, (c) 135°.

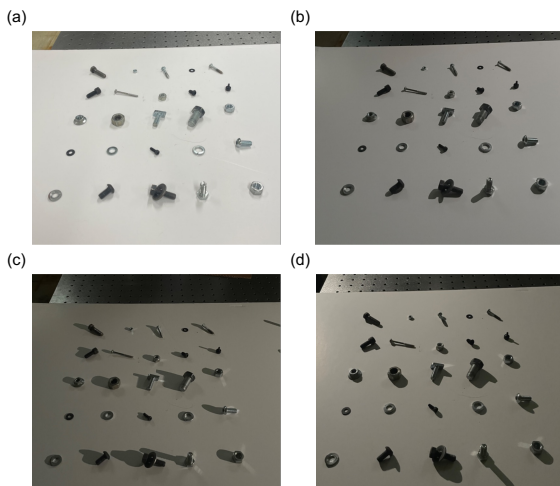


Figure 12. Example of lighting variation in the dataset to enhance robustness of model training (a) regular lighting (b) reduced lighting (c) lighting at 225° (d) 45°.

5.2. Object-detection model design and implementation

The object-detection model is implemented using the YOLOv5m architecture for real-time semantic recognition of near-field objects. Among the 5,000 synthetic image, 3,500 are used for training, 500 for validation and 1,000 are used for testing. The model is initialized from pretrained yolov5m.pt weights and fine-tuned for 50 epochs with a batch size of 16.

After training, the model achieves a mean average precision (mAP@0.5) of 100 percent on the validation set, demonstrating strong generalization across all ten object categories.

For deployment, the trained network is compiled to the HALIO 8L format and executed on a Raspberry Pi 5 equipped with a Raspberry Pi AI HAT+. The inference pipeline includes image capture and resizing, tensor packing for HALIO 8L, hardware-accelerated inference, and CPU-side post-processing. The system operates at a sustained rate of approximately 25 frames per second. This configuration allows immediate object recognition and responsive decision output according to action table in Table 1. The object-detection approach enables the system to distinguish small objects from human hands or shoes of similar height, supporting more context-aware decision making in manufacturing environments.

5.3. Results

The trained YOLOv5m model was evaluated on the synthetic dataset and verified using real images captured by the AMR-mounted camera. Quantitative results are summarized in Table 4. The detector achieved a mean average precision (mAP@0.5) of 100% and mAP@0.5:0.95 of 99% across ten object categories. Precision and recall values for all classes exceeded 0.85, indicating reliable identification of both small and large parts commonly present on the factory floor. On-device inference using the Raspberry Pi AI HAT+ achieved an average latency of 40 ms per frame, corresponding to a sustained input rate of 25 frames per second.

Representative qualitative results are shown in Figure 13, which illustrates accurate detection of a human foot and a metallic component within the near-field region. The model correctly localized and classified both objects with high confidence, demonstrating its ability to distinguish human body parts from surrounding industrial materials. These results confirm that the object-detection module provides consistent and real-time semantic awareness, supporting the decision-making layer for near-field safety monitoring.

Table 4. Per-class performance of YOLOv5m object detection model

Class	Precision	Recall	F1 Score
Bolt	0.98	0.92	0.95
Nut	0.97	0.90	0.94
Washer	0.96	0.88	0.92
Connector	0.95	0.89	0.92
Wire	0.94	0.87	0.90
Screwdriver	0.93	0.85	0.89
Wrench	0.94	0.87	0.90
Marker	0.91	0.82	0.86
Zip tie	0.92	0.83	0.87
Allen key	0.95	0.86	0.90
mAP@0.5	1.00		

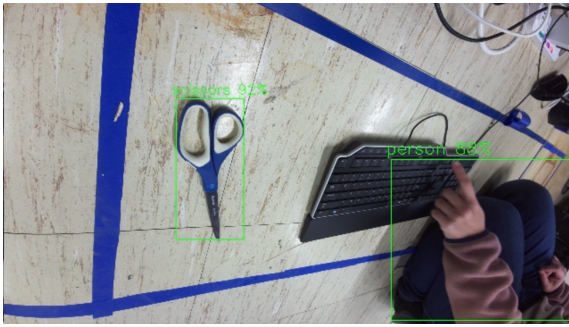


Figure 13. Example inference results of the YOLOv5m model showing accurate detection of a human and tool within the near-field region.

6. Discussion

This section discusses the comparative characteristics of the three approaches in terms of system cost, computational efficiency, and application suitability. The analysis highlights how sensing complexity increases alongside functional capability, offering practical guidelines for selecting approaches in manufacturing environments.

6.1. Cost and system complexity

The cost and complexity of the system scale with the sensing capability of each approach. Table 5 compares the three near-field perception approaches in terms of cost, performance, and capabilities. Approach 1 uses a low-cost Class 3R laser diode, a camera module, and a Raspberry Pi 5, totaling approximately \$207, making it the most economical configuration. Approach 2 employs identical hardware but introduces geometric alignment requirements between the laser and camera for light-displacement calibration, maintaining the same cost but slightly higher structural complexity. Approach 3 removes the laser entirely and instead deploys the YOLOv5m model using a Raspberry Pi 5 with a HALIO AI HAT+ hardware acceleration and the same camera module, totaling approximately \$257. While its hardware cost is moderately higher, this configuration achieves the most advanced sensing capability by adding semantic interpretation and the ability to execute the complete action table described in Table 1. The increase in overall cost and system complexity is therefore directly correlated with the intelligence and flexibility of the system.

6.2. Time efficiency and computational performance

The computational performance and system delay is important to real-time warning system. The performance results in Table 5 show that all three approaches maintain real-time operation on the Raspberry Pi 5 platform. Approaches 1 and 2 operate at 50 frames per second with latencies of 40 ms and 45 ms, respectively, allowing immediate cutoff or displacement analysis without perceptible delay. The minor latency increase in Approach 2 arises from the pixel-shift computation required to

calculate height displacement. Approach 3, accelerated by the HALIO AI HAT+, processes frames at 25 frames per second with an average latency of 40 ms. Setup effort follows a similar hierarchy: Approach 1 required approximately twenty minutes for mechanical alignment and threshold adjustment, Approach 2 required about one hour for camera and light height calibration, and Approach 3 was operational within ten minutes once the trained model was uploaded. These results demonstrate that the AI-based approach, while computationally heavier, offers the shortest setup and most scalable deployment process.

6.3. Applicability and limitations

Table 5 compares the cost, performance, and capabilities of the three proposed perception methods. Each method has specific operational constraints that define its ideal application domain. Approach 1 is suitable for low-cost binary cutoff detection, where the primary goal is to determine whether any object interrupts the light curtain. However, it cannot classify or size objects and therefore cannot follow the predefined action table. Approach 2 extends geometric sensing capability by introducing height estimation based on light displacement. This enhancement allows partial differentiation between small debris and larger obstacles, providing additional geometric context to near-field perception. The experimental results achieve a 17.8 mm RMSE in height prediction. The accuracy can be further improved through refined image processing, particularly to enhance estimation performance on reflective objects. Despite this improvement, it remains unable to reliably distinguish between a small tool and a human hand of similar height and suffers from reduced accuracy on reflective surfaces. Approach 3 overcomes these limitations by providing full semantic understanding of the scene, achieving 100 percent mAP@0.5 accuracy and mapping each detection to the appropriate response category in the action table. The trade-offs include sensitivity to lighting conditions and dependence on class coverage within the trained dataset.

In summary, these three-tier approaches form a sequence of increasing cost, intelligence, and adaptability: from binary cutoff detection to geometry-aware estimation and finally to full semantic perception. Manufacturers can select the most suitable solution according to safety, performance, and budget requirements.

6.4. Future work

Each approach presents opportunities for improvement and further study. For Approach 1, a straightforward improvement is to install an additional camera on the opposite side of the AMR to capture the laser line from two perspectives. This dual-view configuration would compensate for perspective distortion near the far end of the projection, reduce the pixel-to-millimeter resolution loss, and improve the detection of thin or low-profile objects. Combining the two views could also allow limited tri-

Table 5. Comparison of cost, performance, and capabilities across three near-field perception approaches

Approach	Setup time (min)	Frame rate (FPS)	Latency (ms)	Capability	Main limitations
1	20	50	40	Detects presence only (binary cutoff)	Cannot classify or size objects; thin objects at far end may be missed; subject to Class 3R safety policy
2	60	50	45	Estimates object height	Sensitive to reflective surfaces and far-end distortion; cannot distinguish human parts from small tools
3	10	25	40	Full semantic classification and action-table execution	Lower FPS; limited to trained classes; affected by low lighting

angulation to estimate object width without increasing computational cost.

For Approach 2, future work will focus on enhancing the reliability of height estimation through improved calibration and multi-wavelength projection [15, 16]. Employing structured patterns rather than a single line could provide greater spatial redundancy and reduce sensitivity to surface reflectivity.

Approach 3 offers the greatest potential for system-level expansion. Future research will extend the object-detection framework to a multimodal perception architecture that combines visual detection with geometric and temporal cues from Approaches 1 and 2. This fusion would allow the system to retain the speed and simplicity of laser-based sensing while leveraging semantic context for robust decision-making under variable lighting and partial occlusion. Additional directions include deploying lightweight Transformer-based backbones to improve energy efficiency [17], expanding domain adaptation to enable rapid model transfer across different plant environments [18, 19], and exploring continuous learning on the AMR for adaptive perception in dynamic manufacturing settings [20, 21].

Beyond the current hardware setup, a promising direction is the integration of high-precision 3D scanners with excellent near-field sensing capabilities. Although such scanners are widely used in manufacturing quality inspection [22, 23, 24], their application to near-field safety enhancement for AMRs remains limited. The fine-scale 3D information has the potential to support more accurate decision-making, though associated computational challenges may need to be addressed [25]. Moreover, while multi-modal sensing fusion has shown effectiveness in a range of recent applications, including safety-critical autonomous systems [26], contextual object detection [27], and real-time multi-modal detection [28], its potential for improving near-field safety perception in AMRs is still underexplored. Future work could investigate complementary sensing modalities, such as 3D point clouds, thermal, infrared, and ranging sensors, to enhance near-field collision avoidance and safety performance across diverse manufacturing environments.

7. Conclusion

This study presented a three-tier framework for near-field perception on AMRs, spanning geometric and semantic percep-

tion within a scalable architecture. The first approach provided a simple and binary solution for real-time laser line cutoff detection. The second approach extended capability by estimating object height from laser-stripe shifts, adding geometric context with minimal computational overhead. The third method further advanced perception by introducing semantic understanding through embedded AI hardware, supporting category-based decision-making aligned with a predefined action table.

Experimental results confirmed real-time performance across the three methods on a Raspberry Pi 5 platform, with frame rates ranging from 25 to 50 FPS. Together, these methods demonstrate a scalable sensing hierarchy for AMRs that balances precision, cost, and interpretability. The proposed framework offers a practical foundation for intelligent near-field perception to enable safe operations of AMRs in manufacturing environments.

Acknowledgements

The authors gratefully acknowledge the financial support of General Motors (GM) and the technical assistance provided by Zhongyou Zhao and Weitian Zhou from GM during the experimental phase of this study.

References

- [1] M. Lackner, D. Wurhofer, M. Tscheligi, Review of automated mobile robots in intralogistics, *Journal of Industrial Information Integration* (2024).
- [2] M. Dhandu, B. A. Rogers, S. Hall, E. Dekoninck, V. Dhokia, Reviewing human-robot collaboration in manufacturing: Opportunities and challenges in the context of industry 5.0, *Robotics and Computer-Integrated Manufacturing* 93 (2025) 102937.
- [3] G. Wang, C. Zhang, S. Liu, Y. Zhao, Y. Zhang, L. Wang, Multi-robot collaborative manufacturing driven by digital twins: advancements, challenges, and future directions, *Journal of Manufacturing Systems* 82 (2025) 333–361.
- [4] V. Villani, F. Pini, F. Leali, C. Secchi, Survey on human–robot collaboration in industrial settings, *Mechatronics* 61 (2018) 1–13.
- [5] P. A. Lasota, T. Fong, J. A. Shah, A survey of methods for safe human–robot interaction, *Foundations and Trends in Robotics* 5 (2017) 261–349.
- [6] W. Li, Y. Hu, Y. Zhou, D. T. Pham, Safe human–robot collaboration for industrial settings: a survey, *Journal of Intelligent Manufacturing* 35 (2024) 2235–2261.

- [7] L. C. Sousa, Y. M. Silva, V. B. Schettino, T. M. Santos, A. R. Zachi, J. A. Gouvêa, M. F. Pinto, Obstacle avoidance technique for mobile robots at autonomous human-robot collaborative warehouse environments, *Sensors* 25 (2025) 2387.
- [8] A. Bonci, P. D. Cen Cheng, M. Indri, G. Nabissi, F. Sibona, Human-robot perception in industrial environments: A survey, *Sensors* 21 (2021) 1571.
- [9] A. Saha, B. C. Dhara, 3d lidar-based obstacle detection and tracking for autonomous navigation in dynamic environments, *International Journal of Intelligent Robotics and Applications* 8 (2024) 39–60.
- [10] H. Liu, C. Wu, H. Wang, Real time object detection using lidar and camera fusion for autonomous driving, *Scientific Reports* 13 (2023) 8056.
- [11] D. Gualda, J. Ureña, J. C. Garcia, E. Garcia, J. Alcalá, Simultaneous calibration and navigation (scan) of multiple ultrasonic local positioning systems, *Information Fusion* 45 (2019) 53–65.
- [12] T. Nesti, S. Boddana, B. Yaman, Ultra-sonic sensor based object detection for autonomous vehicles, in: *Proceedings of the IEEE/CVF conference on computer vision and pattern recognition*, 2023, pp. 210–218.
- [13] Blender Foundation, Blender – a 3d modelling and rendering package, <https://www.blender.org>, 2024.
- [14] R.-S. Mei, G. Li, S. Jia, L. Huang, L.-W. Shih, J. Arinez, J. Abell, C. Shao, Synthetic data generation in smart manufacturing applications: A systematic review, *SSRN Electronic Journal*, preprint. Available at SSRN: <http://dx.doi.org/10.2139/ssrn.5726804> (2025).
- [15] H. Chang, D. Li, X. Zhang, X. Cui, Z. Fu, X. Chen, Y. Song, Real-time height measurement with a line-structured-light based imaging system, *Sensors and Actuators A: Physical* 368 (2024) 115164.
- [16] B. Lyu, C. Chen, J. Wang, C. Li, W. Zhang, Y. Feng, F. Dong, B. Zhang, Z. Zeng, Y. Wang, et al., Multi-wavelength structured light based on metasurfaces for 3d imaging, *Nanophotonics* 13 (2024) 477–485.
- [17] Y. Li, H. Mao, R. Girshick, K. He, Exploring plain vision transformer backbones for object detection, in: *European conference on computer vision*, Springer, 2022, pp. 280–296.
- [18] M. Khodabandeh, A. Vahdat, M. Ranjbar, W. G. Macready, A robust learning approach to domain adaptive object detection, in: *Proceedings of the IEEE/CVF international conference on computer vision*, 2019, pp. 480–490.
- [19] Z. Fatima, S. Zardari, M. H. Tanveer, Advancing industrial object detection through domain adaptation: A solution for industry 5.0, in: *Actuators*, volume 13, MDPI, 2024, p. 513.
- [20] K. Shmelkov, C. Schmid, K. Alahari, Incremental learning of object detectors without catastrophic forgetting, in: *Proceedings of the IEEE international conference on computer vision*, 2017, pp. 3400–3409.
- [21] J. Wang, X. Wang, Y. Shang-Guan, A. Gupta, Wanderlust: Online continual object detection in the real world, in: *Proceedings of the IEEE/CVF international conference on computer vision*, 2021, pp. 10829–10838.
- [22] Y. Yang, Z. Dong, Y. Meng, C. Shao, Data-driven intelligent 3d surface measurement in smart manufacturing: Review and outlook, *Machines* 9 (2021) 13.
- [23] M. Biehler, Y. Sun, S. Kode, J. Li, J. Shi, Plural: 3d point cloud transfer learning via contrastive learning with augmentations, *IEEE Transactions on Automation Science and Engineering* 21 (2023) 7550–7561.
- [24] R.-S. Mei, C. H. Conway, M. V. Bimrose, W. P. King, C. Shao, Deep learning of 3d point clouds for detecting geometric defects in gears, *Manufacturing Letters* 41 (2024) 1324–1333. 52nd SME North American Manufacturing Research Conference (NAMRC 52).
- [25] M. Engelcke, D. Rao, D. Z. Wang, C. H. Tong, I. Posner, Vote3deep: Fast object detection in 3d point clouds using efficient convolutional neural networks, in: *2017 IEEE International Conference on Robotics and Automation (ICRA)*, IEEE, 2017, pp. 1355–1361.
- [26] Y.-T. Chen, J. Shi, Z. Ye, C. Mertz, D. Ramanan, S. Kong, Multimodal object detection via probabilistic ensembling, in: *European Conference on Computer Vision*, Springer, 2022, pp. 139–158.
- [27] Y. Zang, W. Li, J. Han, K. Zhou, C. C. Loy, Contextual object detection with multimodal large language models, *International Journal of Computer Vision* 133 (2025) 825–843.
- [28] M. Sharma, M. Dhanaraj, S. Karnam, D. G. Chachlakis, R. Ptucha, P. P. Markopoulos, E. Saber, Yolors: Object detection in multimodal remote sensing imagery, *IEEE Journal of Selected Topics in Applied Earth Observations and Remote Sensing* 14 (2020) 1497–1508.